# Interaction of Ferromagnetic Shape Memory Alloys and RGD Peptides for Mechanical Coupling to Cells: from Ab Initio Calculations to Cell Studies

*Mareike Zink, Florian Szillat, Uta Allenstein, and Stefan G. Mayr**

**Due to their magneto-mechanical coupling and biocompatibility, Fe-Pd based ferromagnetic shape memory alloys are a highly promising materials class for application as contact-less magneto-mechanical transducers in biomedical environments. For use in cell and tissue actuators or strain sensors, sufficient adhesion to mediate strains clearly constitutes a prerequisite. As the RGD sequence is the most important binding motif for mammalian cells, which they express to facilitate adhesion, the potential of RGD coatings to achieve this goal is explored. Employing large-scale density functional theory calculations the physics of bonding between RGD and Fe-Pd surfaces, which is characterized by coordinate bonds of O and N atoms to Fe, accompanied by electrostatic contributions, is clarified. Theoretical predictions on adhesion, that are confirmed experimentally, suggest RGD as suitable strain mediator to Fe-Pd surfaces. On the cell side, favorable adhesion properties of RGD-coated Fe-Pd are manifested in cell morphology and spreading behavior. Demonstrating that the adhesion forces between RGD and Fe-Pd exceed those exerted by cells to the RGD coating, as well as traction forces acting onto integrin bonds, the findings pave the way for novel type of applications as cell and tissue actuator or sensor within the areas of tissue engineering and regenerative medicine.**

## 1. Introduction

Ferromagnetic shape memory (FSM) alloys[1] constitute a novel class of functional materials with strong magneto-mechanical coupling, that have attracted significant interest for engineering applications in the past years. Yielding magnetically switchable strains up 10%[2] and, vice versa, magnetization changes upon straining, they can be regarded as perfect candidates for biomedical actuation and sensing. This particularly holds true, as they can be reversibly operated at constant (body) temperature. Temperature changes to induce a shape change, as in conventional shape memory alloys (such as NiTi),[3,4] are not required. Besides their FSM properties, these alloys still can be operated as conventional shape memory alloys, though, and also show such important properties as pseudo("super")elasticity and –plasticity. The "prototype" FSM material, Ni-Mn-Ga, has been demonstrated to be cytotoxic,[5] while the Fe-Pd FSM system[6] proved to be biocompatible in cell and simulated body fluid tests.[7] Membranes of the latter alloy are thus highly promising candidates for use in biomechanical actuators or sensors for shear strains and/or volume dilations of several percent, and could find their way into in vivo applications, including drug delivery systems or adaptive implants.

Clearly such envisioned use relies on sufficient mechanical coupling between the FSM surface and living cells. Generally, adhesion of cells to the extracellular matrix and other substrates determines migration of cells, proliferation and tissue regeneration. Loss in adhesion can lead to aniokis (detachment induced apoptosis) due to focal adhesion kinase inactivation.[8] Moreover, the performance of implant materials in vivo depends on the ability of the surrounding tissue to adhere to the biomedical device such as hip prostheses to ensure osteointegration[9–11] or to synthetic vascular grafts to promote endothelial attachment.[12] Cellular adhesion can be promoted by coating FSM substrates with extracellular matrix (ECM) proteins, e.g., fibronectin or vitronectin that are recognized by integrin receptors on the cellular surface.[13] However, as discovered in 1984 by Pierschbacher and Ruoslahti, the arginine-glycine-aspartic (RGD) sequence of fibronectin, and many other adhesion proteins, is a recognition site, which can bind to $\alpha 5\beta 1$ and $\alpha v\beta 3$ integrins.[14,15] RGD peptides, which are not specifically designed to selectively bind to certain receptors, can be recognized by all five $\alpha$v intergins, two $\beta 1$ and $\alpha$IIb$\beta 3$ integrins on the cell surface,[16] which link the ECM to the cytoskeleton.[17]

Although coatings composed of RGD-containing ligands can promote bioactivity and osseointegration,[11,18–21] only

Dr. M. Zink, U. Allenstein
Soft Matter Physics Division
Faculty of Physics and Earth Sciences
University of Leipzig
04103 Leipzig, Germany
F. Szillat, U. Allenstein, Prof. S. G. Mayr
Leibniz-Institut für Oberflächenmodifizierung e.V.
Permoserstr.15, 04318 Leipzig, Germany
Translationszentrum für Regenerative Medizin
Universität Leipzig, 04103 Leipzig, Germany
E-mail: stefan.mayr@iom-leipzig.de
Prof. S. G. Mayr
Fakultät für Physik und Geowissenschaften
Universität Leipzig, 04103 Leipzig, Germany

**DOI: 10.1002/adfm.201201789**

immobilized RGD peptides support cell adhesion in vitro and can effectively mediate strains between cells and Fe-Pd membranes, while dissolved RGD molecules within the culture medium inhibit cell attachment.[13] To this end, the interaction of the substrate material with the RGD peptides is of major importance when functionalizing the surface for improved cell attachment. Although integrins, such as $\alpha 5\beta 1$ and $\alpha v\beta 3$, bound to RGD are quickly recycled within approximately 30 minutes,[22] RGD peptides in solution would immediately block the receptors again. Thus, only surfaces that strongly bind RGD peptides prevent detachment and promote cell adhesion and migration. Since cells express RGD containing proteins themselves to adhere to substrates, the interaction of RGD with Fe-Pd is supposed to determine cellular morphology, spreading behavior, as well as proliferation and motility.

Motivated by this background, our present study first employs large-scale ab initio density functional theory (DFT)[23] calculations to clarify the physics of bonding between RGD peptides and Fe-Pd surfaces. We demonstrate, that coordinate bonds preferentially form between the O/N and Fe atoms of RGD peptides and Fe-Pd surfaces, respectively, which ensures stable attachment and the capability of transferring stresses between cells and substrates. Based on these findings, we propose an easy-to-use single-step RGD coating strategy of Fe-Pd FSM alloys, that yields functionalized surfaces for mechanical transduction to cells. While on the Fe-Pd side this is experimentally verified by delamination tests that show excellent agreement with our DFT predictions in terms of adhesion, in vitro cell assays with RGD-coated Fe-Pd substrates confirm favorable attachment also on the cell side. Here the expression of focal adhesion sites is quantitatively analysed and compared to cells on uncoated surfaces, as well as control cells on glass and RGD-coated glass. Thus, our finding can be regarded as a key step towards novel applications of Fe-Pd based FSM alloys in biological sciences and regenerative medicine.

## 2. Results

### 2.1. Physics of Bonding of RGD Peptides to Fe-Pd Membranes

When heading for applications of FSM membranes in cell straining or sensing applications, excellent mechanical coupling between cells and FSM membranes clearly constitutes a prerequisite. While interaction between the presently employed RGD peptide coating layer and cell integrins is established to be rather strong on a biophysics energy scale,[24] bonding conditions at the RGD peptide–Fe-Pd FSM interface have been much less clear up to now, particularly as the disordered Fe-Pd alloy surface involves a chemically highly reactive (Fe) and a greatly inert (Pd) component, respectively. DFT based total energy calculations[23] are clearly the method of choice to gain new insights by yielding quantitative ab initio predictions, including the electronic and structural ground states as well as the physics of bonding. It is worth noting here, that for systems as large as the present this constitutes a numerically highly demanding challenge requiring extensive use of massively parallel supercomputers.[25] In fact, as realistic empirical potentials and

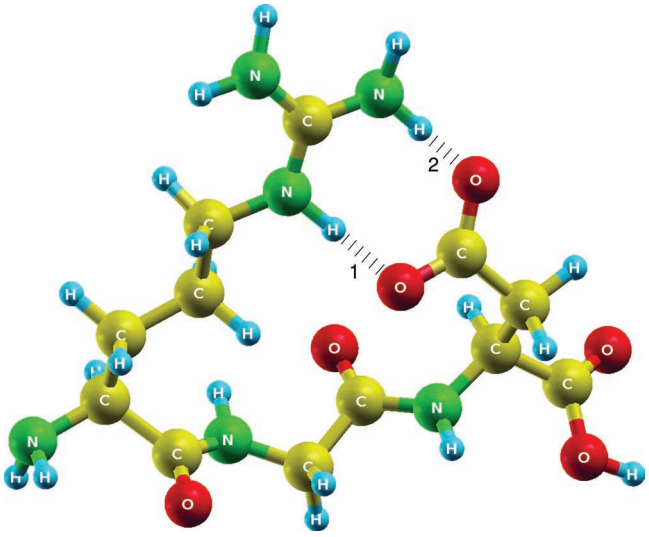


**Figure 1.** Fully relaxed atomic configuration of the RGD peptide, as predicted by the present DFT calculations. Cyclic RGD forms by proton transfer from O to N (1), accompanied by occurrence of two hydrogen bonds (1) and (2).

force fields, which are computationally much less demanding within, e.g., classical molecular dynamics simulations, do exist for biological systems and metals but not for combinations of both worlds, the use of an ab initio approach as DFT virtually remains precondition for reliable theoretical predictions.

As first aspect in our DFT study, we address the electronic and structural ground states of freestanding Fe-Pd membranes and isolated RGD peptides. Due to the applied boundary conditions (Section 5) the former are guaranteed to reside within the face-centered-tetragonal (fct) martensite phase (that is required for magnetic actuation), while, primarily due to size differences between Fe and Pd ions and the presence of surfaces, ionic structural relaxations prove to be highly relevant in reaching the overall ground state. An extensive account on the resulting structural, energetic and thermodynamic properties of Fe-Pd membranes has been published recently.[26] As for the isolated RGD peptide, careful structural relaxation of the initial textbook structure[27] results in a cyclic conformation (**Figure 1**), which is characterized by i) a proton transfer from O to an opposing N accompanied by a change of the adjacent C bond to a double and single bond, respectively (as marked in Figure 1) and ii) establishment of two hydrogen bonds (1 and 2 in Figure 1) with one of them occurring in the location of the proton transfer. Clearly these two hydrogen bonds are responsible for the energetic preference of the observed cyclic conformation.

The cyclic RGD peptide in its relaxed vacuum configuration is subsequently aligned parallel to the Fe-Pd surface and brought into six different locations chosen randomly along two different relaxed Fe-Pd surfaces. The initial distance was chosen so as to maximize binding energy each,as probed with numerous self-consistent electronic structure runs at fixed ion positions. During subsequent careful ionic relaxation of these six Fe-Pd/RGD configurations with the techniques described in Section 5, the energy is further minimized, yielding configurations with binding energies in the range from –3.49 to –4.45 eV

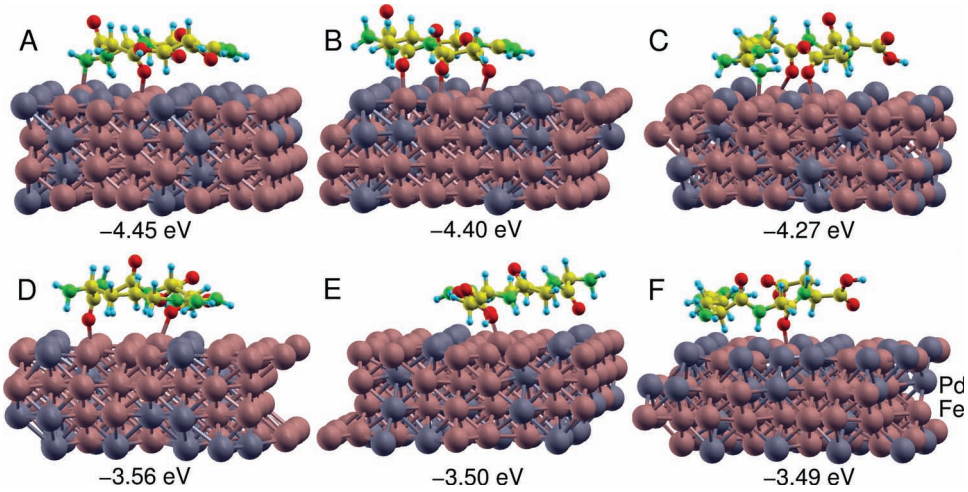


**Figure 2.** Bond characteristics between the RGD peptide and the Fe-Pd ferromagnetic shape memory alloy at different locations along the surface. Coordinate bonds preferentially establish between Fe and O, as well as Fe and N, while Pd is never observed to get involved in bonding. The corresponding binding energies are given below the configurations.

(**Figure 2**). Employing the average (–3.95 eV) as typical binding energy between a single RGD peptide and the Fe-Pd surface and using the typical RGD dimension (1.2 nm × 1.2 nm), we thus obtain 0.4 J/m$^2$ as an estimate for the typical binding energy between an RGD film and Fe-Pd.

While it is primarily the RGD peptide, which, due to its softness in comparison to the Fe-Pd membrane, reveals structural readjustments in the course of energy minimization, it is very instructive to look a little deeper, i.e., atomically resolved, into the physics of bonding. To identify possible bonding partners between RGD and Fe-Pd, we first employed a bond length criterion and have drawn a chemical bond in Figure 2, where the sum of their covalent radii[28] exceeds their actual distance. As we will demonstrate below, this criterion reliably identifies the key locations of coordinate bonding between RGD and Fe-Pd, while additional weaker bonding also occurs between delocalized electrons in Fe-Pd and RGD, respectively. Clearly, on the RGD side the constituents with unbonded electron pairs closeby (i.e., O and N) engage in bonds with Fe atoms of the FSM membrane surface, while C and Pd were never observed to get involved. Due to the random occupation of the FSM membrane surface ("random solid solution") with Fe and Pd, where thus only Fe sites are "hot spots" for binding to RGD, this implies highly heterogeneous binding characteristics between RGD and Fe-Pd. In most favorable binding configurations the loci and spacings between the Fe atoms on the surface will be compatible with O and N of the RGD polypeptide, while deviations from this perfect configuration will first lead to stresses within RGD and ultimatively in a reduction of the number of bonds to Fe-Pd. This is reflected by a reduction of the RGD–Fe-Pd absolute binding energy, as observed in Figure 2.

As for bonding geometry, it is furthermore very instructive to evaluate the bond angles occurring at the RGD/Fe-Pd interface. While N is always found to be coordinated as nearly perfect regular tetrahedron, the C-O-Fe bond angles scatter between 126.6° and 151.8° with an average value of 139° ± 9°.

To explore the character of the atomic bonds between RGD and Fe-Pd more thoroughly and, after all, confirm presence and types of chemical bonds on hard grounds, we have explored the electronic densities of states (DOS) of freestanding Fe-Pd membranes, isolated RGD peptides as well as RGD peptides attached to Fe-Pd membranes (**Figure 3**). Clearly the spin-polarized band structure of Fe-Pd and discrete molecular orbitals of RGD are discernible prior to aggregation, which show significant energetic overlap within the lower half of the conduction band of Fe-Pd. Due to the atomic proportions, the DOS after aggregation is severely dominated by Fe-Pd (Figure 3).

To assess the physics of bonding it is therefore very instructive to contemplate the density of states of the whole system projected onto atomic orbitals of the bonding partners on the RGD and Fe-Pd sides, viz. the Fe-N and Fe-O bonds

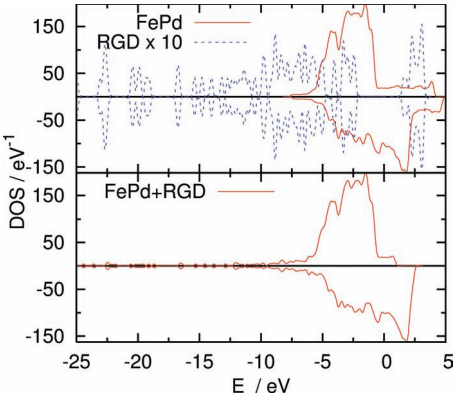


**Figure 3.** Electronic densities of states for freestanding Fe-Pd membranes and isolated RGD peptides, as well as total electronic densities of states after aggregation, exemplarily for configuration Figure 2A. Energies are given relative to the Fermi energy; positive and negative values correspond to spin up and spin down electrons, respectively.

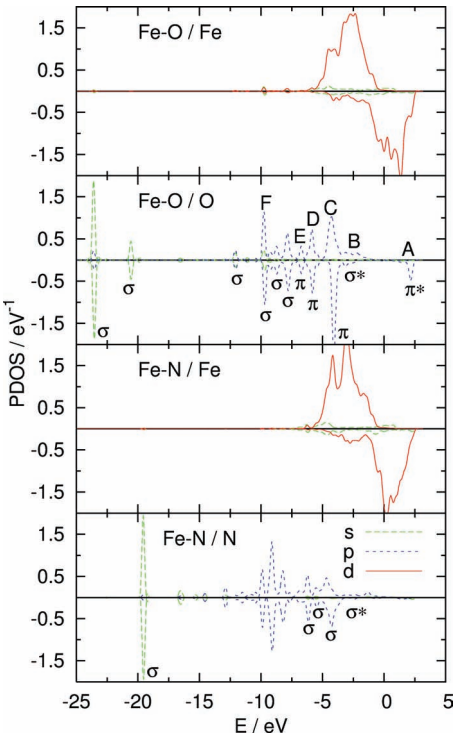


**Figure 4.** Projected densities of states onto Fe and O atomic orbitals of the Fe-O bond as well as onto the Fe and N atomic orbitals of the Fe-N bond between the RGD peptide and Fe-Pd membrane (exemplarily for configuration of Figure 2A). The type ($\sigma$ or $\pi$-like) and character (bonding/antibonding ($^*$)) of the bonds is also given. Energies are given relative to the Fermi energy; positive and negative values correspond to spin up and spin down electrons, respectively.

highlighted in Figure 2. We first focus on a representative Fe-O bond (**Figure 4**, upper half), where a careful analysis[30] yields multiple resonances between the sp hybridized O and the Fe 4s and 3d bands. To address the character (bonding/antibonding ($^*$)) and type ($\sigma/\pi$) of bonding, the local densities of states are integrated along individual O resonance peaks, and plotted as isosurfaces. While a representative selection of the latter is presented in **Figure 5**, a more extensive evaluation of the integrated local density of states (ILDOS)[31] for every resonance between Fe and O yields the classification ($\sigma/\pi/\sigma^*/\pi^*$) given in Figure 4. For the Fe-N bond, on the other hand, resonances are primarily apparent between the sp$^3$-hybridized N and Fe 3d bands, which are similarly classified into $\sigma$ and $\sigma^*$ bonds. In both cases, viz. O-Fe and N-Fe bonds, all but one resonance below the Fermi energy are bonding. This large majority of bonding orbitals thus is the physical origin of the rather strong adhesion of the RGD peptide to Fe-Pd.

Besides the O-Fe and N-Fe bonds that have been discussed up to now, we also detected additional resonances between delocalized electrons in Fe-Pd and RGD, viz. in locations without ions on the symmetry axis of bonding. These delocalized-electron-mediated bonds proved to be of $\sigma$-type throughout; one example is included in Figure 5D.

As the presently dominating O-Fe and N-Fe bonds clearly have a large similarity to dipolar bonds in metal-organic complexes, where charge transfer can play an important role, we explored the net charge transfer between the RGD peptide and Fe-Pd membrane upon aggregation. Employing the Lowdin[32] and Bader[33] concepts (**Table 1**), charge transfer was determined to be lower than 0.237e, or 2%, throughout. Although charge transfer is thus of minor importance in the present case, we did detect a slight shift of charge within Fe-Pd surface from the O and N bonding sites to other regions. This can be interpreted as electrostatic attraction by image charges in course of the large electronegativity of O and N, respectively.

### 2.2. Experimental Quantification of Adhesion

Among the detailed DFT predictions above, the presumably most relevant quantity from an experimental point of view is given by the binding energy (0.4 J/m$^2$) of the RGD peptide to the Fe-Pd membrane surface. Experimentally, the latter is addressed by a delamination test, viz. by peeling the RGD peptide film off the Fe-Pd membrane, while measuring the required work. Employing a cantilever-based laser beam deflection dilatometer (Section 5, Figure S1 (Supporting Information); for a detailed account see Supporting Information, Section B), the peel-off stress (defined as the maximum tensile stress in peel-off experiments) is determined to be (0.7 ± 0.4) mN/mm$^2$, while we estimate for the adhesion energy (0.5 ± 0.3) J/m$^2$.

### 2.3. Wettability with Water Before and After Coating

As adhesion of cells to substrates is crucially affected by their wettability with water, it is very instructive to explore the impact of the RGD coating with respect to this: While the contact

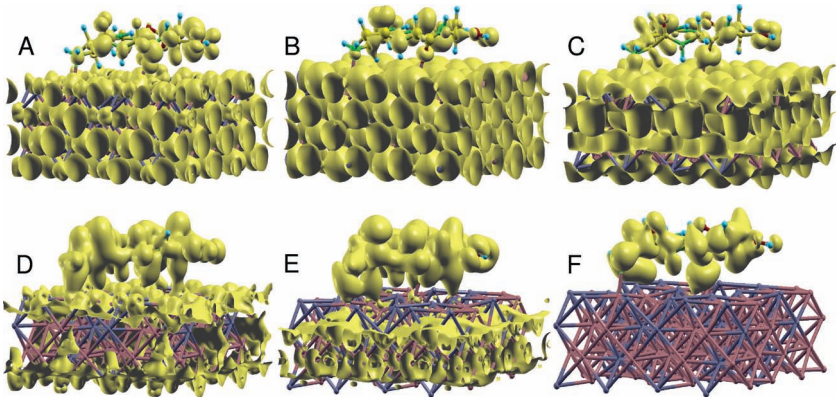


**Figure 5.** Local density of states, integrated around the peaks A–F (marked in Figure 4), exemplarily selected for the ionic configuration shown in Figure 2A. The isosurfaces of A–F correspond to isovalues of 0.13, 0.67, 0.54, 0.017, 0.0035 and 0.0067 1/Å$^3$ for A–F, respectively. While antibonding $\pi$ and $\sigma$-like orbitals are discernible in A and B, respectively, $\pi$ and $\sigma$-like bonding is observed in C–E and F, respectively.

**Table 1.** Charge transfer (in units of e) between the RGD peptide and the Fe-Pd membrane upon attachment. According to Lowdin[32] and Bader[33] analyses, charge transfer is less than 2% throughout.

| | RGD attached | Fe-Pd attached | RGD only | Fe-Pd only |
|---|---|---|---|---|
| Lowdin | 134.34 | 1091.73 | 134.349 | 1091.57 |
| Bader | 136.237 | 1103.77 | 136.00 | 1104.00 |

angle[34] of water on an untreated $Fe_7Pd_3$ surface was measured as $\theta_{H2O} = 104° \pm 3°$, an additional RGD coating changes wetting behavior significantly. A strong tendency of wetting within a few seconds indicates super-hydrophilicity here.

### 2.4. Cell Morphology and Adhesion

To study the influence of RGD coating on the morphology and adhesion behavior of living cells, NIH 3T3 fibroblasts were seeded onto uncoated and RGD-coated Fe-Pd substrates and incubated for 4 days. Subsequently, the F-actin cytoskeleton was stained with phalloidin to visualize structure and morphology of the cells, while focal contacts were marked with anti-vinculin. Confocal laser scanning microscopy imaging revealed that cells spread well with normal heterogeneous, fibroblast cell shapes (Supporting Information Figure S2 and **Figure 6**).

To quantify these observations, the average projected area of the cells was calculated, yielding a value of (1780 ± 177) μm$^2$ on uncoated Fe-Pd (Figure 6). Furthermore, the dimensionless shape factor $\sigma = 4\pi A/p^2$, the normalized ratio of the cell area $A$ and the square of the perimeter $p$, was analyzed to determine the cellular shape in terms of circularity in more detail. A shape factor close to 1 indicates circular cell areas, while values close to zero are found for elongated objects with the shape of a straight line. On uncoated Fe-Pd surfaces, a shape factor of 0.45 ± 0.03 was obtained (Figure 6E), corroborating our visual observations of irregular cell morphologies and polarized shapes. The F-actin stress fibers were found to be well pronounced within the cells as an indicator of spread cells (Figure 6A). The area of the focal contacts in terms of the area of anti-vinculin stained contact sites was measured with image analysis software. We found that a surface cell area of (125 ± 28) μm$^2$ exhibited a fluorescent signal of the adhesion sites (Figure 6E), which relates to a focal contact density (fraction of cell area occupied by focal contacts) of 4.9% ± 0.6%.

After coating the Fe-Pd substrates with RGD, fibroblasts well adhered and spread on the coated membranes, while on average the cell size in terms of projected area was reduced by 45% to (995 ± 24) μm$^2$ (Supporting Information Figure S2B, Figure 6). In contrast, the shape factor hardly increased to 0.49 ± 0.01. In addition, the focal contact density remained almost unchanged within the error bars with 4.7% ± 0.5%. Thus, the total fraction of cell area covered by focal contacts ((78 ± 12) μm$^2$) decreased by the same factor as the projected cell area. Visual inspections revealed F-actin stress fibers spanning the entire cell body as seen for cells on untreated surfaces (Figure 6B).

To compare these findings with cells on other well-established solid substrates, NIH 3T3 cells were seeded on untreated and RGD-coated glass coverslips and analyzed, as described

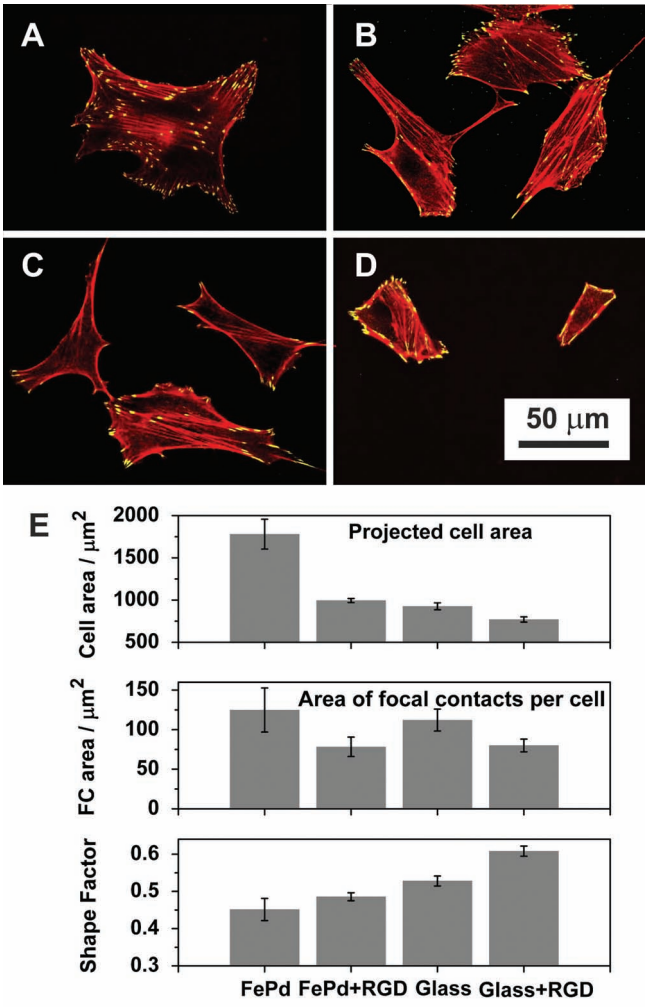


**Figure 6.** Confocal laser scanning microscopy pictures of NIH 3T3 fibroblasts on A) Fe-Pd and B) RGD-coated Fe-Pd substrates. Control measurements with cells on C) glass coverslips and D) RGD-coated glass. The red signal shows the actin cytoskeleton and the green signal the focal contact sites. E) Projected cell areas, total areas of focal contacts per cell and calculated shape factors for cells cultured on Fe-Pd, RGD-coated Fe-Pd films, as well as control measurements on glass and RGD-coated glass. The error bars give the standard deviation.

before. As can be seen in Figure 6C, cells on uncoated glass spread but were smaller compared to fibroblasts on Fe-Pd substrates with average projected areas of (926 ± 41) μm$^2$, while the F-actin stress fibers were clearly visible (Figure 6C and Supporting Information Figure S2C). The cell morphology was more rounded, which is reflected in the shape factor of 0.53 ± 0.01. However, the total area covered by focal contacts was hardly reduced compared to uncoated Fe-Pd substrates with a total value of (112 ± 14) μm$^2$; this results in a clear increase in focal contact density to 7.6% ± 0.7% due to smaller cell areas.

After coating the glass coverslips with RGD, the projected cell area decreased even further to (769 ± 31) μm$^2$, less than half the size on the untreated Fe-Pd surface (Figure 6D,E and Supporting Information Figure S2D). The cells became even

more rounded with a shape factor of 0.61 ± 0.01. Interestingly, the total area covered by focal contacts (80 ± 8) μm$^2$ was identical to the focal contact area of RGD coated Fe-Pd (Figure 6E). However, the focal contact density doubled to 10.6% ± 0.1% due to differences in projected cell areas. Actin stress fibers were hardly seen for cells on coated glass substrates as visualized in Figure 6D. In the bottom line, the smallest and most spherical cells were determined on the RGD coated glass substrates.

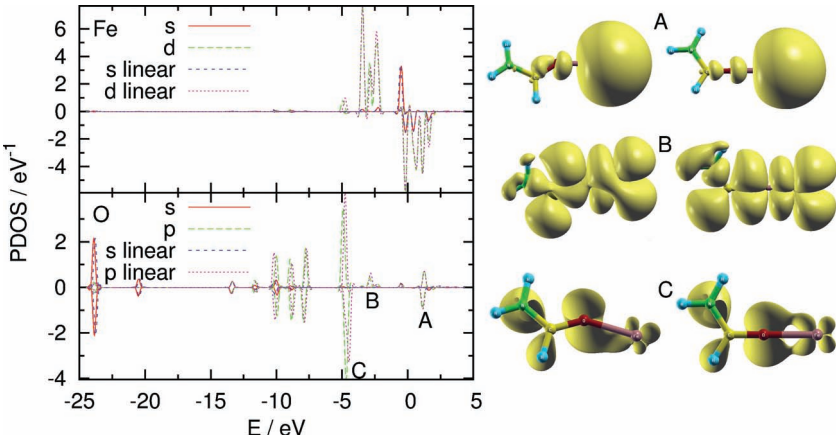


**Figure 7.** Origin of the bond angle of ≈147° in the formamide iron complex: the projected density of states on the atomic orbitals of the bond constituents, Fe and O, for tilted and linear bond alignment, reveal distinct resonances, that are visualized as isosurfaces of the corresponding integrated densities of states (isovalues A: 0.02, B: 0.00028 and C: 0.0056 Å$^{-3}$). For linear alignment, resonances B and C reveal antibonding $\pi$ character, while structural relaxation towards a 147° inclination of Fe vs. O results in bonding $\sigma$-like character by appropriate "overlapping" of O $p_y$ and Fe $d_{xy}$ orbitals, besides a further delocalization of the C–O $\pi$ bond into the Fe $d_{xz}$ orbital. Evaluation of the O orbital-specific PDOS yields sp-hybridization of O.

## 3. Discussion

Cells generally adapt to their chemical and physical environments. The presently investigated "hard" substrate is characterized by smooth surfaces and mechanical strengths exceeding those cells can sense due to mechanotransduction[35,36] by orders of magnitudes. Cellular behavior is thus highly influenced by other factors, such as chemical composition, surface energy, electric charges, and corrosion resistance. Coatings can tailor these properties and improve cellular attachment. Especially proteins occurring within the extracellular matrix of the mammalian body are highly relevant for bioactivity enhancement, since they contain the RGD recognition motif for cellular attachment via integrins and formation of focal adhesion complexes.[37]

To wrap up the bonding characteristics between the RGD polypeptide and the Fe-Pd FSM alloy surface, analysis of our extensive DFT calculations clearly demonstrates presence of chemical bonds. The latter primarily occur between Fe and O or N atoms on the Fe-Pd and RGD sides, respectively, but also in a weaker fashion between delocalized states within RGD and the Fe-Pd band. While thus most relevant aspects of bonding have been clarified, the C-O-Fe bond angles, however, remain a puzzle. Depending on the detailed bonding conditions they are found around 139° ± 9°. To obtain deeper insight into the underlying electronic origins, we chose to stick with the subsystem that mediates bonding between RGD and Fe-Pd, viz. the formamide-iron complex. Performing a structural relaxation of this complex results in a C-O-Fe bond angle of 147°, similar to the one observed in our RGD/Fe-Pd system. To obtain a clue about the electronic origins of this relaxation, we compared the electronic structure of a relaxed with an unrelaxed (bond angle of 180°) system (**Figure 7**). The PDOS onto the Fe and O orbitals reveals three key resonances in the relaxed and unrelaxed cases, the ILDOS of which are visualized as isosurfaces on the rhs. in Figure 7. Comparing the structurally unrelaxed to the relaxed configuration, it becomes clear that by bending the C-O-Fe bond the system is capable of establishing a $\sigma$-bond instead of a $\pi$-bond in resonance C, while obtaining bonding orbitals instead of antibonding in resonance B. Both changes of electronic structure due to ionic relaxation towards a 147° bond angle result in reduction of total energy,and thus make it the preferred configuration. As for the C-O-Fe bond in the RGD/Fe-Pd system, things are just the same, i.e., presence of the 3d band instead of discrete 3d levels does not change the physics of bonding fundamentally here.

As for a quantitative comparison of the bonding energies predicted by DFT with our experiments, we obtain excellent agreement (0.4 J/m$^2$ vs. (0.5 ± 0.3) J/m$^2$, respectively), which, in fact, is far from trivial. In particular the experimentally performed delamination tests are commonly prone to systematic errors, as correct determination of the adhesion energies via mechanical integration requires absence of dissipation per se. Complications particularly arise from non-linear deformations within the coating, which generally affect peel force (see e.g., ref. [38] and references therein for details). The presently observed agreement thus can be regarded as indication that reversibility is greatly fulfilled. This can be understood in terms of the bonding energy between RGD and Fe-Pd, which is high enough to prevent occurrence of thermally activated viscous-like creep effects on the lab timescale at ambient temperatures (and thus certainly also on the time scale determined by the velocity of the step motor of 12 μm/s, corresponding to a strain rate at the RGD/Fe-Pd interface of some $10^4$ s$^{-1}$). This delamination rate obviously is still slow enough to remain close to quasistatic equilibrium throughout. With a peak strain of some 5% of the Fe-Pd membrane, this means that in the whole anticipated operation regime (from static to some kHz), the RGD/Fe-Pd coupling remains close to quasistatic equilibrium and thus sufficiently mediates strains to cells.

Biocompatibility assessments already showed that cells can adhere and proliferate on the surface of Fe-Pd substrates.[7] However, the interaction of cells with different substrate materials is still a matter of debate, and contributions of surface and interaction energies to the ability of cells to adhere and form focal contacts are unknown. Expression of RGD containing proteins by the cells themselves support adhesion, while furthermore the adhesion of these proteins on the substrate is

triggered by interaction and surface energy differences. Only when bonding of the RGD-containing coating is strong enough to prevent delamination of the RGD layer from the Fe-Pd surface during cellular adhesion and motion, bioactivity of the substrate can be enhanced.[39–41]

Our in vitro assessments demonstrate that NIH 3T3 fibroblasts spread well on uncoated Fe-Pd substrates. To compare our cell culture results with the behavior of cells on well-established substrates, we furthermore investigated the interaction of fibroblasts with uncoated glass coverslips. It turned out, that cells were much larger and heterogeneous in shape on Fe-Pd samples. The total cell areas covered by focal contacts are almost identical for cells on Fe-Pd and glass substrates, which might be triggered by surface energy differences that promote cell spreading on Fe-Pd.

Investigations on the interaction of bioglasses composed of $SiO_2$, $Na_2O$, CaO and $P_2O_5$ showed that large quantities of silicon, as present in glass coverslips, lead to increased proliferation of cells.[42] During mitosis cells round up, exhibit an increased shape factor and decrease the projected area on the substrate surface as seen in our experiments. Additionally, increased surface wettability as observed for glass coverslips with contact angles of ≈51°[43] compared to 104° ± 3° on Fe-Pd also enhances fibroblast proliferation.[44] Thus, accelerated cell division might contribute to the observed finding of smaller and more rounded fibroblasts on glass. Future proliferation assays will focus on a better understanding of wettability and materials-induced cell division.

To understand the decrease in cell size after coating substrates with RGD, the interaction of RGD with the environment needs to be taken into account, viz. 1) the substrate material interaction with the RGD coating by establishing chemical bonds as discussed above and 2) the bonding of RGD to the integrin receptors of cells. Thus, two competing interactions act on RGD. While cells bind to RGD, they spread and prepare for migration. If the interaction between the RGD ligand and the substrate is lower than maximum forces cells exert on their binding sites during spreading and migration, the RGD peptide will get ripped-off the surface. As a result cells cannot spread and migrate anymore, round up and decrease in size. At a final step apoptosis will be induced if adhesion of cells is completely hampered.

To quantify forces of cellular adhesion from our investigations, we assume an adhesion site spacing of 60 nm.[45,46] Thus, about 300 integrin receptors per $\mu m^2$,[36] and up to 23.400 RGD-integrin bonds could be involved in cell-substrate adhesion on the observed focal contact area of 78 $\mu m^2$ on the RGD-coated Fe-Pd film. This value corresponds to up to 23% of all possible $\alpha5\beta1$ integrin receptors on the surface of a fibroblast cell - in good agreement with ref. [47]. However, it is expected that the RGD peptides rupture from the surface during spreading and migration of cells only, if the forces exerted by cells to the focal contact site are large enough. During retraction, myosin-II develops forces in the range of 1–10 nN/$\mu m^2$ determined by traction force measurements of fibroblasts,[36,48,49] corresponding to up to 0.03 nN per integrin bond and even 0.10–0.17 nN for early adhesion units as reported by Moore et al.[36] For the RGD-FePd interaction, our DFT simulations yielded maximum bonding strengths of 1.03 nN and 1.13 nN between O-Fe and N-Fe, respectively, as determined for H terminated formamide-iron and ammonia-iron complexes, which constitute subgroups of RGD attached to Fe-Pd. As additional bonds between delocalized electrons and ionic contributions due to image charges in Fe-Pd are not included, these constitute lower limits. Thus, the "weak-link" in the adhesion binding site during spreading and migration of cells is not the RGD adhesion to the Fe-Pd substrate, but the RGD-integrin complex itself, even when taking into account that 3–5 integrins are required to couple to the cytoskeleton and form a focal contact complex.[50] To this end, pure RGD peptides constitute a biomimetic coating for Fe-Pd even without chemically advanced processes of peptide immobilization.

On the other hand, weaker bonding and more mobile RGD peptides might be expected for the interaction of RGD and glass because here cells are smaller and more rounded. Furthermore, possible dissolution of RGD during cell culture must be taken into account to understand why cells have reduced projected cell and focal contact areas after RGD coating. Dissolution behavior depends on how strong the RGD is bound, which for RGD layer thicknesses beyond one monolayer certainly decreases as a function of distance from Fe-Pd and in surface proximity, respectively. A thick coating layer thus might increase the amount of dissolved RGD molecules which can bind to integrin receptors. Although recycling of RGD-bonded $\alpha5\beta1$ integrin receptors in NIH 3T3 fibroblasts occurs within 30 min,[22] integrins will get blocked again immediately. Other integrin receptors cannot compensate for the decreased number of contact sites forming the adhesion bonds to the substrate. In fact, $\alpha5\beta1$ is the major binding site for adhesion strength.[24,35]

The observed morphological changes might also correlate with cell motility. Static, non-moving fibroblasts are usually well spread with a large projected area and many stress fibers. In contrast, motile cells tend to exhibit a round cell body with a leading edge, the lamellipodium and a trailing tail.[51] During migration cells develop less focal adhesions than static cells. Thus, future studies will focus on migration of cells on Fe-Pd substrates and the effect of coatings on cell motility.

## 4. Conclusions

To conclude, we have studied for the first time the physics of bonding between RGD peptides and metal surfaces for the biomedically promising example of the Fe-Pd ferromagnetic shape memory alloy from first principles. A decent interaction of RGD coatings with the substrate material, which is mediated by coordinate bonds between N/O and Fe on the RGD and Fe-Pd sides, respectively, and accompanied by electrostatic contributions, opens the venue for improved in vivo performance of FSM-based medical devices and allows in vitro applications as cell actuators and sensors. Because 10–20% of all joint prostheses fail within 15 years after implantation, a deeper understanding on how cells couple via RGD-integrin sites to metallic substrates generally lays the foundations for new surface processing concepts to expand lifespan and reduce replacement surgeries to a minimum.

## 5. Experimental Section

Additional details are included in the Supporting Information.

*DFT Calculations*: DFT[23] based total energy calculations were conducted employing a plane wave basis set in combination with

ultrasoft pseudopotentials[52,53] using a customized version of the PWSCF code.[54] Dispersion forces were included within the semiempirical DFT-D approach,[55,56] while utilizing the spin-polarized general gradient approximation according to Perdew-Burke-Ernzerhof (PBE). Atomic disorder was treated within a special quasirandom structure (SQS) approach,[57] which was structurally relaxed using the Broyden-Fletcher-Goldfarb-Shanno (BFGS) scheme, before determining final energies, charge densities and (projected) densities of states.

*Delamination Tests and Adhesion*: After depositing (120.0 ± 0.5) nm Fe-Pd onto a (250 ± 10) µm thick Cirlex CL-HN polymer foils, the latter were coated with RGD peptides and employed in a home-built cantilever deflection dilatometer. Setup, an exemplary measurement, model assumptions for data evaluation and possible sources of error are discussed in detail in the Supporting Information, Section B. While more than eight peel-off experiments on the RGD/Fe-Pd system under various conditions were performed, peel-off stresses and works of delamination shown in the present work were based on three independent measurements in the optimized setup (see Supporting Information, Section B), peeling with a speed of 12 µm $s^{-1}$.

*Contact Angle Measurements*: Wettability of pure and RGD-coated Fe-Pd, respectively, with water was assessed by means of a commercial contact angle measuring system (DSA2, Kruess GmbH, Germany) using 4 µL water drops. Uncertainty was determined from the standard deviation of at least three independent drops measured ten times each.

*RGD Coating Protocol*: In order to coat 1.0 $cm^2$ thin FePd films with RGD peptides, 2 µg RGD (Abbiotec, Cat. No. 350362) was dissolved in 2 µL Millipore ultrapure water, and subsequently diluted with 70 µL phosphate buffered saline (PBS). For cell experiments, the substrate was incubated for 60 min at 37 °C, humidified air and 5% $CO_2$. Subsequently, remaining solution was removed from the surface and cells were seeded immediately. For adhesion and surface wettability measurements, substrates were kept at 37 °C for 50 min, the remaining solution was removed and substrates were kept at 37 °C for additional 10 min to obtain the required dry surfaces.

*Cell Tests*: Interaction of cells with coated and uncoated Fe-Pd thin films was investigated with NIH 3T3 embryonic mouse fibroblasts. Cells were cultured for 4 days on Fe-Pd and RGD-coated Fe-Pd films with Dulbecco's modified Eagle's medium, high glucose, L-glutamine, supplemented with 10% calf serum and penicillin/streptomycin at 37 °C, humidified air and 5% $CO_2$. Millipore's Actin Cytoskeleton and Focal Adhesion Staining Kit was used to study F-actin and focal contact organizations within the cells. TRITC-conjugated phalloidin was employed to map F-actin filaments and vinculin monoclonal antibody together with FITC-conjugated Goat Anti-Mouse IgG for focal contact sites. Cells were imaged with confocal laser scanning microscopy and compared to reference cells cultured on glass and RGD-coated glass coverslips under same conditions.

## Supporting Information

Supporting Information is available from the Wiley Online Library or from the author.

## Acknowledgements

The authors are indebted to Prof. Dr. Dr. h.c. B. Rauschenbach and Prof. Dr. J. A. Käs for general support. The authors gratefully acknowledge financial support from the German Science Foundation (DFG) - Project BIOSTRAIN, as well as the German Federal Ministry of Education and Research (BMBF, PTJ-BIO, 0315883). Part of the work was performed within the Leipzig Graduate School of Natural Sciences "Building with Molecules and Nano Objects" (BuildMoNa), established within the German Excellence Initiative by the German Science Foundation (DFG).

Received: July 1, 2012
Revised: September 18, 2012
Published online: October 16, 2012

[1] K. Ullakko, J. K. Huang, C. Kantner, R. C. O'Handley, V. V. Kokorin, *Appl. Phys. Lett.* **1996**, *69*, 1966.
[2] A. Sozinov, A. A. Likhachev, N. Lanska, K. Ullakko, *Appl. Phys. Lett.* **2002**, *80*, 1746.
[3] W. J. Buehler, J. V. Gilfrich, R. C. Wiley, *J. Appl. Phys.* **1963**, *34*, 1475.
[4] J. Pfetzing-Micklich, M. F.-X. Wagner, R. Zarnetta, J. Frenzel, G. Eggeler, A. E. Markaki, J. Wheeler, T. W. Clyne, *Adv. Eng. Mater.* **2010**, *12*, 13.
[5] L. L. Stepan, D. S. Levi, E. Gans, K. P. Mohanchandra, M. Ujihara, G. P. Carman, *J. Biomed. Mater. Res. A* **2007**, *82A*, 768.
[6] R. D. James, M. Wuttig, *Philos. Mag. A* **1998**, *77*, 1273.
[7] Y. Ma, M. Zink, S. G. Mayr, *Appl. Phys. Lett.* **2010**, *96*, 213703.
[8] F. Schatzmann, R. Marlow, C. H. Streuli, *J. Mammary Gland Biol. Neoplasia* **2003**, *8*, 395.
[9] D. M. Dohan Ehrenfest, P. G. Coelho, B.-S. Kang, Y.-T. Sul, T. Albrektsson, *Trends Biotechnol.* **2010**, *28*, 198.
[10] T. Albrektsson, C. Johansson, *Eur. Spine J.* **2001**, *10*, S96.
[11] T. A. Petrie, J. E. Raynor, C. D. Reyes, K. L. Burns, D. M. Collard, A. J. García, *Biomaterials* **2008**, *29*, 2849.
[12] A. M. Seifalian, A. Tiwari, G. Hamilton, H. J. Salacinski, *Artif. Organs* **2002**, *26*, 307.
[13] E. Ruoslahti, *Annu. Rev. Cell Dev. Biol.* **1996**, *12*, 697.
[14] J. Ivaska, J. Heino, *Cell Tissue Res.* **2010**, *339*, 111.
[15] M. D. Pierschbacher, E. Ruoslahti, *Nature* **1984**, *309*, 30.
[16] J. D. Humphries, A. Byron, M. J. Humphries, *J. Cell Sci.* **2006**, *119*, 3901.
[17] P. Kanchanawong, G. Shtengel, A. M. Pasapera, E. B. Ramko, M. W. Davidson, H. F. Hess, C. M. Waterman, *Nature* **2010**, *468*, 580.
[18] B. Elmengaard, J. E. Bechtold, K. Søballe, *Biomaterials* **2005**, *26*, 3521.
[19] D. Ferris, G. Moodie, P. Dimond, C. W. Giorani, M. Ehrlich, R. Valentini, *Biomaterials* **1999**, *20*, 2323.
[20] K. M. Hennessy, W. C. Clem, M. C. Phipps, A. A. Sawyer, F. M. Shaikh, S. L. Bellis, *Biomaterials* **2008**, *29*, 3075.
[21] S. Rammelt, T. Illert, S. Bierbaum, D. Scharnweber, H. Zwipp, W. Schneiders, *Biomaterials* **2006**, *27*, 5561.
[22] D. P. White, P. T. Caswell, J. C. Norman, *J. Cell Biol.* **2007**, *177*, 515.
[23] P. Hohenberg, W. Kohn, *Phys. Rev.* **1964**, *136*, B864.
[24] P. Roca-Cusachs, N. C. Gauthier, A. del Rio, M. P. Sheetz, *Proc. Natl. Acad. Sci. USA* **2009**, *106*, 16245.
[25] For the present study some $10^6$ CPU hours on a state-of-the-art supercomputer.
[26] S. G. Mayr, *Phys. Rev. B* **2012**, *85*, 014105.
[27] As e.g., available from the National Center for Biotechnology Information - PubChem Compound Database; CID=104802, http://pubchem.ncbi.nlm.nih.gov/summary/summary.cgi?cid=104802&loc=ec_rcs (accessed December 2010).
[28] Chosen as 0.399 Å, 0.8085 Å, 0.7875 Å, 0.7665 Å, 1.47 Å and 1.47 Å for H, C, N, O, Fe and Pd, respectively. See ref. [29].
[29] A. Kokalj, *Comp. Mater. Sci.* **2003**, *28*, 155.
[30] Employing also projections onto individual p and d orbitals, respectively.
[31] By plotting numerous isosurfaces at different isolevels.
[32] P.-O. Lowdin, *J. Chem. Phys.* **1950**, *18*, 365.
[33] R. Bader, *Atoms in Molecules: A Quantum Theory (International Series of Monographs on Chemistry)*, Oxford University Press, Oxford, UK **1994**.
[34] The contact angle $\theta$ is given by $\theta = (180° - \theta_{inside})$ with $\theta_{inside}$ measured inside the liquid drop.
[35] B. Geiger, J. P. Spatz, A. D. Bershadsky, *Nat. Rev. Mol. Cell Biol.* **2009**, *10*, 21.
[36] S. W. Moore, P. Roca-Cusachs, M. P. Sheetz, *Dev. Cell* **2010**, *19*, 194.

[37] T. Shemesh, B. Geiger, A. D. Bershadsky, M. M. Kozlov, *Proc. Natl. Acad. Sci. USA* **2005**, *102*, 12383.
[38] A. J. Kinloch, J. G. Williams, in *The Mechanics of Adhesion* (Ed: D.A. Dillard, A.V. Pocius), Elsevier, Amsterdam **2002**, p. 273.
[39] B. T. Houseman, M. Mrksich, *Biomaterials* **2001**, *22*, 943.
[40] D. H. Davis, C. S. Giannoulis, R. W. Johnson, T. A. Desai, *Biomaterials* **2002**, *23*, 4019.
[41] U. Hersel, C. Dahmen, H. Kessler, *Biomaterials* **2003**, *24*, 4385.
[42] A. Hoppe, N. S. Güldal, A. R. Boccaccini, *Biomaterials* **2011**, *32*, 2757.
[43] A. Sklodowaka, M. Wozniak, R. Matlakowska, *Biol. Proced. Online* **1999**, *1*, 114.
[44] G. Altankov, F. Grinnell, T. Groth, *J. Biomed. Mater. Res.* **1996**, *30*, 385.
[45] E. A. Cavalcanti-Adam, T. Volberg, A. Micoulet, H. Kessler, B. Geiger, J. P. Spatz, *Biophys. J.* **2007**, *92*, 2964.
[46] C.-H. Yu, J. B. K. Law, M. Suryana, H. Y. Low, M. P. Sheetz, *Proc. Natl. Acad. Sci. USA* **2011**, *108*, 20585.
[47] D. Boettiger, in *Methods in Enzymology, Volume 426: Integrins* (Ed. D.A. Cheresh), Academic Press, New York **2007**, Ch. 1.
[48] M. Dembo, Y. L. Wang, *Biophys. J.* **1999**, *76*, 2307.
[49] C. G. Galbraith, M. P. Sheetz, *Proc. Natl. Acad. Sci. USA* **1997**, *94*, 9114.
[50] F. Coussen, D. Choquet, M. P. Sheetz, H. P. Erickson, *J. Cell Sci.* **2002**, *115*, 2581.
[51] M. J. Dalby, M. O. Riehle, D. S. Sutherland, H. Agheli, A. S. G. Curtis, *Biomaterials* **2004**, *25*, 5415.
[52] D. Vanderbilt, *Phys. Rev. B* **1990**, *41*, 7892.
[53] A. M. Rappe, K. M. Rabe, E. Kaxiras, J. D. Joannopoulos, *Phys. Rev. B* **1990**, *41*, 1227.
[54] P. Giannozzi, S. Baroni, N. Bonini, M. Calandra, R. Car, C. Cavazzoni, D. Ceresoli, G. L. Chiarotti, M. Cococcioni, I. Dabo, A. Dal Corso, S. de Gironcoli, S. Fabris, G. Fratesi, R. Gebauer, U. Gerstmann, C. Gougoussis, A. Kokalj, M. Lazzeri, L. Martin-Samos, N. Marzari, F. Mauri, R. Mazzarello, S. Paolini, A. Pasquarello, L. Paulatto, C. Sbraccia, S. Scandolo, G. Sclauzero, A. P. Seitsonen, A. Smogunov, P. Umari, R. M. Wentzcovitch, *J. Phys.: Condens. Matter* **2009**, *21*, 395502.
[55] S. Grimme, *J. Comput. Chem.* **2006**, *27*, 1787.
[56] V. Barone, M. Casarin, D. Forrer, M. Pavone, M. Sambi, A. Vittadini, *J. Comput. Chem.* **2009**, *30*, 934.
[57] A. Zunger, S.-H. Wei, L. G. Ferreira, J. E. Bernard, *Phys. Rev. Lett.* **1990**, *65*, 353.